Biogeosciences Discuss., 8, 11255–11284, 2011
www.biogeosciences-discuss.net/8/11255/2011/
doi:10.5194/bgd-8-11255-2011

Biogeosciences Discussions

Oxygen exchange and ice melt measured at the ice-water interface by eddy correlation

M. H. Long[1], D. Koopmans[1], P. Berg[1], S. Rysgaard[2,3], R. N. Glud[2,4,5], and D. H. Søgaard[2,5]

[1]Department of Environmental Sciences, University of Virginia, Charlottesville, Virginia, USA
[2]Greenland Climate Research Centre, Greenland Institute of Natural Resources, Nuuk, Greenland
[3]Centre for Earth Observation Science, CHR Faculty of Environment Earth and Resources, University of Manitoba, Winnipeg, Canada
[4]Scottish Association of Marine Sciences, Oban, Scotland, UK
[5]Southern Danish University and NordCee, Odense M, Denmark

Received: 28 October 2011 – Accepted: 7 November 2011 – Published: 23 November 2011

Correspondence to: P. Berg (pb8n@virginia.edu)

Published by Copernicus Publications on behalf of the European Geosciences Union.

Abstract

This study uses the eddy correlation technique to examine fluxes across the ice-water interface. Temperature eddy correlation systems were used to determine rates of ice melting and freezing, and O_2 eddy correlation systems were used to examine O_2 exchange rates as driven by biological and physical processes. The research was conducted below 0.7 m thick sea ice in mid March 2010 in a southwest Greenland fjord and revealed low average rates of ice melt amounting to a maximum of 0.80 ± 0.09 mm d^{-1} (SE, $n = 31$). The corresponding calculated O_2 flux associated with release of O_2 depleted melt water was less than 13 % of the average daily O_2 respiration rate. Ice melt and insufficient vertical turbulent mixing due to low current velocities caused periodic stratification immediately below the ice. This prevented the determination of fluxes during certain time periods, amounting to 66 % of total deployment time. The identification of these conditions was evaluated by examining the velocity and the linearity and stability of the cumulative flux. The examination of unstratified conditions through velocity and O_2 spectra and their cospectra revealed characteristic fingerprints of well-developed turbulence. From the observed O_2 fluxes, a photosynthesis/irradiance curve was established by least-squares fitting. This relation showed that light limitation of net photosynthesis began at 4.2 µmol photons m^{-2} s^{-1}, and that the algal communities were well-adapted to low-light conditions as they were light saturated for 75 % of the day during this early spring period. However, the sea ice associated microbial and algal community was net heterotrophic with a daily gross primary production of 0.69 ± 0.02 mmol O_2 m^{-2} d^{-1} (SE, $n = 4$) and a respiration rate of -2.13 mmol O_2 m^{-2} d^{-1} (no SE, see text for details) leading to a net primary production of -1.45 ± 0.02 mmol O_2 m^{-2} d^{-1} (SE, $n = 4$). Modeling the observed fluxes allowed for the calculation of fluxes during time periods when no O_2 fluxes were extracted. This application of the eddy correlation technique produced high temporal resolution O_2 fluxes and ice melt rates that were measured without disturbing the environmental conditions while integrating over a large area of approximately 50 m^2 which encompassed the highly variable activity and spatial distributions of sea ice algal communities.

BGD

8, 11255–11284, 2011

1 Introduction

Sea ice associated microbial communities can be an important component of marine polar food webs (Arrigo, 2003) and when sea ice is present it can host 30–65 % of the ecosystem primary production (e.g. Mikkelsen et al., 2008; McMinn et al., 2010). Primary production and phototrophic growth in sea ice is largely limited by the amount of light that transmits through the ice and snow cover (Arrigo, 2003; McMinn et al., 2010). Therefore, production is tightly linked to photosynthetic efficiency, with sea ice algae being well-adapted to low light conditions (Mock and Gradinger, 1999; Kuhl et al., 2001; Rysgaard et al., 2008). O_2 fluxes are commonly used to determine photosynthetic production and respiration in aquatic ecosystems, however, at the ice-water interface these measurements are complicated by the O_2 flux driven by the physical processes of melting and freezing (Glud et al., 2002). Specifically, sea ice formation can cause a release of O_2 supersaturated brines, while sea ice melt can generate a release of O_2 undersaturated melt water (Glud et al., 2002; Rysgaard et al., 2008), confounding O_2 fluxes due to primary production and respiration. Therefore, to estimate the biotic O_2 flux it is necessary to quantify the physical contribution from freezing and melting.

Sampling at the ice-water interface presents a number of challenges for traditional techniques for quantifying primary production and respiration. The techniques presently used to study sea ice primary production sample at either one point on the ice surface or within an ice core, though algal patchiness and activity have been reported to vary across a much wider range (Gosselin et al., 1986; Rysgaard et al., 2001). This may lead to misrepresentation of the actual sea ice environment and requires that many replicates are taken over a large area. A further limitation of conventional methods is their poor resolution of temporal variation, which has limited the studies of short-term variations at the ice-water interface. The ^{14}C tracer method and ^{3}H labeled thymidine approach are the most widely applied techniques to determine primary production and bacteria production in sea ice, respectively. However, both methods are time intensive,

BGD
8, 11255–11284, 2011

making multiple samples and a wide spatial coverage difficult (McMinn and Ashworth, 1998; Søgaard et al., 2010). Both approaches also require melting the ice to evenly distribute the tracers, which grossly changes the natural conditions experienced by the microalgae and bacteria (e.g. nutrient levels, light, and O_2 gradients) (Glud et al., 2002; Rysgaard et al., 2008).

Pulse amplitude modulated (PAM) fluorometry represents a promising alternative to study the primary production of natural communities. However, when PAM is applied to intact ice cores the depth integrated signal is poorly defined and depends on variations in algae biomass as well as the optical properties of the ice (Rysgaard et al., 2001; Glud et al., 2002). Further, to convert the PAM data into carbon (or O_2) equivalents frequent intercalibration to poorly constrained empirical relations are required. Microsensor profiling using both Clark-type O_2 microsensors and O_2 micro optodes has also been used to examine the ice-water O_2 fluxes but suffer from calibration problems due to temperature and salinity interference, spatial micro variability, and the invasiveness of the method which can affect the measuring site (McMinn and Ashworth, 1998; Glud et al., 2002; Mock et al., 2003; McMinn et al., 2007).

Eddy correlation in aquatic environments is a technique typically used for measuring fluxes across the sediment-water interface by correlating high resolution temporal and spatial measurements of velocity and a scalar quantity of interest (Berg et al., 2003). O_2 eddy correlation systems have been used to determine photosynthesis and respiration in muddy marine benthic systems and river bottoms (Berg et al., 2003), sandy sediments (Kuwae et al., 2006; Berg and Huettel, 2008), the deep ocean (Berg et al., 2009), lakes (Brand et al., 2008; McGinnis et al., 2008; Lorrai et al., 2010), hard-bottom arctic substrates (Glud et al., 2010), and seagrass beds (Hume et al., 2011). With the eddy correlation technique, measurements are conducted under true in situ conditions, i.e. without disturbing the surface and under natural light and hydrodynamic conditions (Berg et al., 2003). The technique also integrates over a large surface area, which is typically tens of meters long and a few meters wide (Berg et al., 2007). For these reasons, the technique is ideal for application under sea ice, where fluxes across the

BGD
8, 11255–11284, 2011

ice-water interface can be examined non-invasively. The eddy correlation technique has been used to determine fluxes of momentum, heat, and salt beneath ice (McPhee, 1992; Shirasawa et al., 1997; Widell et al., 2006; McPhee et al., 2008) but has not been previously used to quantify O_2 exchange and thereby production and respiration of sea ice microbial communities. While the technique has been validated for fluxes of heat and salt across the ice-water interface (McPhee, 1992; McPhee et al., 2008) the flux of O_2 across the ice-water interface is complicated by the aforementioned physical processes of ice melting and freezing. In this study we present results obtained with O_2 eddy correlation systems and temperature eddy correlation systems that are used collectively to determine true in situ O_2 exchange rates and thereby non-invasively access the primary production and respiration of sea ice algae communities.

2 Methods

2.1 Site description

Measurements were performed in a small tributary fjord near Kapisigdlit, Greenland from 12–17 March, 2010. The sub-Arctic fjord is located in southwest Greenland and is part of the Nuup Kangerlua Fjord. The fjord was partially covered with ice at a thickness of ~70 cm and a snow cover of ~2 cm over the sampling period. Measurements were conducted 100 m from the ice edge. Air temperatures during the study period ranged from +2.9 °C to −8.8 °C with an average temperature of −3.2 °C. Water depth at the deployment location varied between 40 and 45 m.

2.2 Eddy correlation measurements

Two O_2 eddy correlation systems and two temperature eddy correlation systems were deployed beneath the ice. The O_2 eddy correlation system consists of an acoustic Doppler Velocimeter (ADV) (Nortek AS, Norway) that has been modified to record

BGD
8, 11255–11284, 2011

measurements made with a high-resolution custom-made pA amplifier (Max Planck Institute for Marine Microbiology, Germany) to which a fast responding (<0.2 sec) Clark-type O_2 microelectrode is mounted (Berg and Huettel, 2008; Berg et al., 2009; Hume et al., 2011). The temperature eddy correlation system utilizes a standard ADV coupled to a rapid-response (<0.1 sec) temperature and conductivity sensor (Fast CT sensor, Precision Measurement Engineering, USA) (Crusius et al., 2008). Damage to the conductivity sensors prevented simultaneous measurement of the salt flux.

The systems were positioned under the sea ice by lowering them through a 0.25 by 0.60 m rectangular hole (Fig. 1). This new deployment tactic, compared to traditional tripod mounted systems, was very simple and did not require any diver support. The ADV and sensors were mounted to a stainless steel T rod with the sensors positioned at the edge of the ADV's 1 cm^3 measuring volume that was located 22 to 26 cm below the ice-water interface. Water velocity (x, y, and z components), time, O_2 concentration and temperature were recorded by the ADVs at a frequency of 64 Hz in intervals of 0.25 h. Total measurement periods were typically 24 h long to capture diurnal fluctuations. An O_2 optode (Hach, USA) measured the mean O_2 concentration as a check of the Clark-type O_2 electrodes. Photosynthetically active radiation (PAR) was determined using a self contained cosine-corrected integrating PAR logger (Odyssey, New Zealand) which was deployed just below the ice-water interface.

2.3 Data analysis

Fluxes of O_2 and heat across the ice-water interface were calculated from high resolution measurements of the vertical velocity and either the O_2 concentration or temperature as:

$$\overline{Flux} = \overline{u'_z C'} \quad (1)$$

where u'_z is the instantaneous fluctuating component of the vertical velocity, C' is the instantaneous fluctuating component of the O_2 concentration or temperature, and the bars symbolize averaging over time (Berg et al. 2003). The fluctuating components

BGD
8, 11255–11284, 2011

were separated from the means by Reynolds Decomposition where $u_z' = u_z - \overline{u_z}$ and $C' = C - \overline{C}$ where u_z and C are the instantaneous raw measurements, and the means ($\overline{u_z}$ and $\overline{C}$) were determined by linear least squares fit over each 0.25 h measuring period (Berg et al., 2003). The three-dimensional velocity field was rotated to orient the x-axis into the mean flow direction and to bring the mean perpendicular and vertical velocities to zero to correct for any sensor tilt. The O_2 concentration, temperature, and velocities in each burst were examined carefully for anomalous variations due to sensor malfunctions caused by disturbances of the sensors, for example due to debris floating in the water. Furthermore, the mean current velocity, the cumulative flux of either O_2 or heat, and the spectra of the vertical velocity, the O_2 concentration, and the product of both were used to identify periods with well-developed turbulence under the ice where trustworthy eddy fluxes could be determined (see results and discussion).

The rate of ice melt (h) was calculated from the mean product of u_z' and the turbulent fluctuation in temperature T' as:

$$h = \frac{\overline{u_z' T'} C p_w \rho_w}{\Delta H_f \rho_i} \quad (2)$$

where the bar indicates time averaging, Cp_w is the specific heat capacity of seawater, ρ_w is the density of seawater, ΔH_f is the heat of fusion of ice, and ρ_i is the density of the ice. The numerator of Eq. (2) constitutes the heat flux. For the purposes of a first order calculation of the melt rate we assumed the conduction of heat up through the ice was negligible. That assumption makes the calculated rates represent an upper limit for ice melt. An O_2 flux due to ice melt was determined with the assumption that the melt water from sea ice was anoxic due to the difficulty in determining the O_2 concentration of the melt water. This also results in an overestimate of the O_2 flux due to melting as bulk ice O_2 concentrations were found to range between 40 and 280 µMol L^{-1} at a bulk salinity of 4.6 during the campaign (Tison et al., unpublished data).

Assuming a small constant contribution of ice melt to the total O_2 exchange rate and a constant respiration rate, simple relationships between measured O_2 fluxes,

BGD
8, 11255–11284, 2011

production (P), respiration (R) and the irradiance were developed:

$$O_2\ flux = P - R \tag{3}$$

$$P = P_0(1 - \exp^{(-I/I_k)}) \tag{4}$$

where P_0 is the maximum primary production rate in the photosynthesis to irradiance (P/I) curve for sea ice algae, I is irradiance and I_k is the photoadaptation parameter or the irradiance level at which photosynthesizing organisms begin to become saturated with light (Platt et al., 1980; Smith et al., 1988; Suzuki et al., 1997).

3 Results

Due to periods of low current flow turbulence was not consistently adequate for the mixing of heat and O_2 throughout the water column immediately below the ice. During such periods density stratification developed and restricted vertical mixing across the pycnocline. Generally, well-developed turbulence was found at current velocities greater than 1–2 cm s^{-1}. Figure 2 shows an example of how velocity changed the turbulent transport and mixing under ice. At low current velocities there was insufficient turbulence and little or no vertical mixing occurred, which resulted in the formation of density stratification. As the velocity increased there was a point when the stratification was eroded allowing the water column immediately below the ice to be mixed. This event was evident in large O_2 and temperature fluctuations and it was not used in the flux calculations because of the incompatibility of linear detrending over periods of widely fluctuating O_2 and temperature signals. Furthermore, the mixing of the stratified layer is not indicative of the actual flux at that point in time, and the period leading up to this integrated signal is poorly constrained. The erosion of stratification was followed by a period of stable and linear cumulative flux signal that was suitable for flux determination. Finally, as the velocity and therefore turbulence decreased the stratification was re-established.

BGD
8, 11255–11284, 2011

Stratified conditions were determined by examining the current velocity and the corresponding flux signal. Under low flow conditions the cumulative flux signal became nonlinear and erratic, indicating a weak flux signal. Under high flow conditions a consistent and linear trend in the cumulative flux indicated a strong flux signal. Well-mixed conditions where eddy fluxes could be accurately determined were found 34 % of the time. Unstratified conditions were further examined in the frequency domain through the vertical velocity spectra, where well-mixed conditions and fully developed turbulence was indicated by a characteristic −5/3 slope (Fig. 3a, Kundu and Cohen, 2008). Similarly the O_2 spectra show an initial −5/3 slope at lower frequencies and the expected −1 slope at higher frequencies where viscous forces gain importance (Fig. 3b, Kundu and Cohen, 2008). The normalized cumulative cospectra of O_2 and the vertical velocity (Fig. 3c) also shows the typical fingerprint of turbulent transport of O_2 where eddies with frequencies of less than 0.1 Hz dominate the vertical turbulent transport of O_2. Under well-mixed conditions the fluxes of O_2 and heat were highly reproducible. For example, Fig. 4 shows a typical example of O_2 eddy correlation data at night over 2.5 h, with an average flux of -2.99 ± 0.26 mmol m^{-2} d^{-1} (SE, $n = 10$). The consistent and linear cumulative fluxes indicate a strong flux signal (Fig. 4c).

Consecutively measured O_2 fluxes were grouped into periods when there was sufficient velocity to produce well developed turbulence (Fig. 5). The smallest net O_2 flux into the ice occurred during peak irradiance. No correlation between current direction and the O_2 flux was found ($R^2 = 0.021$, $p = 0.816$, $n = 123$). The white circles in Fig. 5a are the model results determined by simultaneously fitting Eqs. (3) and (4) ($R^2 = 0.923$) to the measured mean fluxes.

The P/I curve (Eq. 3) resulted from the fitting of the eddy correlation data in Fig. 5, with R being the average O_2 flux in the dark ($R^2 = 0.923$, Fig. 6). The maximum P rate was 1.76 ± 0.27 mmol O_2 m^{-2} d^{-1} (SE, $n = 8$) and I_k was 4.2 µmol photons m^{-2} s^{-1} (based on irradiance measured just below the ice-water interface). Using Eqs. (3) and (4) and the measured light values, the 0.25 hr O_2 exchange rates were calculated across 4 days of the study period (Fig. 7). From these model results the daily

BGD
8, 11255–11284, 2011

values of R, gross primary production (GPP), and net primary production (NPP) were calculated as outlined by Cole et al. (2000) and Hume et al. (2011) with the rates weighted by the hours of daylight and darkness and assuming that respiration was the same day and night. This resulted in a value of R of $-2.13\,\mathrm{mmol\,O_2\,m^{-2}\,d^{-1}}$ while GPP averaged $0.69 \pm 0.02\,\mathrm{mmol\,O_2\,m^{-2}\,d^{-1}}$ (SE, $n = 4$), and NPP averaged $-1.45 \pm 0.02\,\mathrm{mmol\,O_2\,m^{-2}\,d^{-1}}$ (SE, $n = 4$). Light saturation (based on I_k) occurred at an average of 1.47 ± 0.09 h (SE, $n = 8$) after first light and before darkness. With an average day length of 11.69 ± 0.24 h (SE, $n = 4$) the bottom ice algal communities were therefore light saturated for 75 % of the day.

The mean heat flux was $2.83 \pm 0.30\,\mathrm{W\,m^{-2}}$ (SE, $n = 31$), giving a calculated rate of ice melt of $0.80 \pm 0.09\,\mathrm{mm\,d^{-1}}$ (SE, $n = 31$) during unstratified conditions. The mean observed temperature of seawater during the measuring period was $-0.05\,^{\circ}\mathrm{C}$ and the salinity 33. The specific heat capacity of the seawater was assumed to be $3.999\,\mathrm{J\,g^{-1}\,^{\circ}C^{-1}}$ and the density was assumed to be $1.026\,\mathrm{g\,cm^{-3}}$ (Fofonoff and Millard, 1983). In our first-order calculation of melting rates we assumed that the entire heat flux towards the sea ice was used to melt pure ice, and thus, neglected any portion of the flux that might have been lost by heat conduction up into the ice interior. As explained above, this leads to an overestimation of the ice melt rate and of the O_2 flux associated with it. Based on this assumption we used a heat of fusion for pure ice of $333.6\,\mathrm{J\,g^{-1}}$ (Harvey, 2010) and a density of ice of $0.917\,\mathrm{g\,cm^{-3}}$ (Eicken, 2003). The average ice melt rates shown in Fig. 8 varies from 0.49 ± 0.11 (SE, $n = 6$) to $0.99 \pm 0.25\,\mathrm{mm\,d^{-1}}$ (SE, $n = 8$). The ice melt rates were not significantly different between each period ($F_4 = 2.040$, $p = 0.111$ at 0.01 level). The O_2 flux that was calculated based on the ice melt rates, through the melting of de-oxygenated ice, averaged $-0.28 \pm 0.03\,\mathrm{mmol\,O_2\,m^{-2}\,d^{-1}}$ (SE, $n = 31$). This flux amounts to less than 13 % of the daily respiration rate derived from fitting Eqs. (3) and (4) to the data in Fig. 5.

The footprint, or the area of the ice surface that contributes 90 % of the measured eddy flux (Fig. 9), was calculated from estimated values of the friction velocity (u*), the surface roughness (z_o), and the measuring height as described by Berg et al. (2007).

BGD
8, 11255–11284, 2011

This calculation revealed a value of u* of $0.098 \pm 0.007\,cm\,s^{-1}$ (SE, $n = 20$) and a hydraulically smooth ice surface with a z_0 of 0.023 ± 0.002 cm (SE, $n = 20$) (see Berg et al., 2007 for details). The oval shaped footprint was about 2.8 m wide by 67 m long with a point of maximum flux contribution at 3.2 m upstream from the eddy correlation instrument (Fig. 9).

The level of anisotropy in the turbulent flow below the sea ice, as reflected in the ratios between the eddy diffusivities (Ex, Ey, and Ez) in the x, y, and z directions, was estimated as described by Berg et al. (2007). Figure 10 shows that anisotropy was clearly evident (Ex/Ez = 6.2 ± 1.0, Ey/Ez = 3.8 ± 0.5, Ez/Ez = 1 ± 0.0; SE, $n = 5$).

4 Discussion

The eddy correlation technique is in many respects superior to traditional flux methods (Berg et al., 2003; Kuwae et al., 2006; Berg and Huettel, 2008) and this study conducted at the ice-water interface further exhibits the adaptability and advantages of the technique. The first measurements of O_2 eddy correlation fluxes at the ice-water interface presented here are controlled by ice melt, and to a much larger extent, the biological activity of the microbial communities. However, the ice-water interface also produces conditions that must be addressed when sampling eddy correlation ice-water fluxes such as low current velocities, density stratifications, and instrument deployment. Despite this, the eddy correlation technique is well suited for flux measurements at the ice-water interface and has previously been applied and validated for momentum, heat, and salt fluxes (McPhee, 1992; Shirasawa et al., 1997; Widell et al., 2006; McPhee et al., 2008).

Measured O_2 exchange rates across the ice-water interface do not directly represent primary production and respiration, as physical processes may also contribute to the exchange. These physical processes include the release of O_2 supersaturated brine during freezing or the release of O_2 undersaturated water during melting (Glud et al., 2002; Rysgaard et al., 2008). Although these physical processes only contributed a

BGD
8, 11255–11284, 2011

minor portion of the total O_2 flux in this study, this will not always be the case. Heat fluxes can be measured and translated into melting rates, but the total ice O_2 concentration as well as the fraction of the measured heat flux that is conducted up into the ice rather than melting it must be determined to calculate the associated O_2 flux.

The release of melt or brine flows may also cause stratification immediately below the ice and therefore a careful examination of the state of turbulence and mixing below the ice-water interface is required. The eddy correlation technique assumes that the dominant form of vertical transport is turbulent mixing. Therefore, the technique may produce inaccurate results at very low current velocities when there is insufficient turbulence. Ice freeze and melt may also cause convection to occur, which has been reported as a problem for measuring O_2 fluxes from profiles generated with microelectrodes (Glud et al., 2002; McMinn et al., 2010). However, with the eddy correlation technique these convective processes are included in measurements, and with the concurrent determination of ice melt rates we can estimate the net O_2 flux due to primary production and respiration.

The lack of vertical mixing under low-flow conditions allowed density stratification to build up immediately below the ice due to ice melt (Fig. 2). This stratification caused the effects of the flux to be confined within the stratified layer near the ice, as evidenced by the large pulse in the signal when the stratification was later eroded (Fig. 2). As a result, accurate fluxes could only be derived when the vertical mixing due to turbulent flow was strong enough to erode and prevent density stratifications. The mean current velocity provided a benchmark for determining when stratification would occur, and this was further evaluated by examining the cumulative flux signal, as little or no flux was recorded during periods of weak turbulence, while stable and linear cumulative fluxes were derived during periods of well-developed turbulence (Fig. 2). The presence of well-developed turbulence was also examined through the spectra of the vertical velocity and the O_2 concentration (Fig. 3a and b). The presence of the characteristic −5/3 slope of the spectra is typical for well-developed turbulence (Kundu and Cohen, 2008). The cospectra of the vertical velocity and O_2 concentration was also

BGD
8, 11255–11284, 2011

examined to determine the frequency of the turbulent eddies that contributed to the flux. For example, in Fig. 3c the contributing eddies had frequencies less than 0.1 Hz, suggesting that mostly larger eddies where vertically mixing the upper water column.

An examination of the eddy diffusivities revealed that the turbulent mixing below the ice was clearly anisotropic as expected in flows near solid boundaries (Fig. 10). The relatively small ratio between the longitudinal (E_x) and vertical (E_z) eddy diffusivity of 6:1 suggests that the water column was fully mixed at least within the upper meters below the ice-water interface. If stratification had been present it would reduce the vertical mixing and therefore give a much larger ratio. For comparison, a ratio of 12:1 was found for a 1 m deep river that was fully vertically mixed (Berg et al., 2007). However, we stress that both the strength and depth of the density stratification are highly dynamic properties that change across time, and that intermittent low-flow current conditions represent a challenge for eddy correlation measurements across the ice-water interface.

The footprint of the eddy correlation technique is very large compared to that of other flux methods (Berg et al., 2007) and is expected to integrate most variability commonly observed at the ice-water interface (McMinn and Ashworth, 1998; Rysgaard et al., 2001). It has been suggested that to include all horizontal variations in light, algal biomass and algal activity it is necessary to measure across distances of 20 to 100 m (Gosselin et al., 1986; Rysgaard et al., 2001; Søgaard et al., 2010). Figure 9 shows the size of the footprint to be over 60 m long, and therefore it integrates over most of this variability. However, given the narrow width of the footprint its composition will change with even a small change in current direction. This variability can easily be determined by examining the correlations between the fluxes and the current direction, and in this study none were found ($R^2 = 0.021, n = 166$).

BGD
8, 11255–11284, 2011

Given the small difference between the mean seawater temperature and its freezing point, low rates of ice melt were expected. Throughout the study period low ice melt was observed (Fig. 8), and the measured O_2 exchange rates indicated a net consumption of O_2 (Fig. 5), which may be due to both the consumption by organisms and to a lesser degree the melting of deoxygenated ice crystals (Glud et al., 2002; Rysgaard and Glud, 2004). Specifically, the O_2 flux associated with ice melting was shown to be less than 13 % of the average daily respiration rate (see Figs. 5 and 8). This calculated potential O_2 flux due to melting assumes that all of the heat flux goes to ice melting and that melt water from the ice is anoxic. The O_2 concentration of water released during melting remains an uncertainty, especially considering that brine channels may advect O_2 depleted or enriched water from anywhere within the ice. The ice also had a significantly lower temperature than that of the water column (McGinnis et al., in progress) and therefore the conduction of heat into the colder ice likely accounted for some heat flux without causing melt. Considering these uncertainties we were able to put an upper limit on how much ice melt could affect the total O_2 flux. Thus, this maximum O_2 flux due to ice melt rates cannot account for any significant differences in fluxes during the study period. However, it is expected that physical processes during ice growth and melting during other periods of the year may greatly affect the O_2 exchange and could potentially exceed the biological signal.

The O_2 flux showed a strong correlation to light (Fig. 5) as GPP reduced the net flux of O_2 toward the ice during the day. However, at all times the ice was net heterotrophic which has been observed by others (Rysgaard and Glud, 2004; Rysgaard et al., 2008). The calculation of GPP uses the standard convention that the daytime and nighttime respiration rates are equal, as it is not possible to separate the daytime respiration and production. However, this may lead to an underestimate of daytime respiration due to the stimulation of respiration by the release of photosynthates (Fenchel and Glud, 2000; Glud et al., 2009).

The P/I curve established through model fitting (Figs. 5 and 6) revealed that the ice algae were well adapted to low light conditions with an I_k of about 4 µmol photons

BGD
8, 11255–11284, 2011

$m^{-2}\,s^{-1}$. This is supported by many other studies that show sea ice algae to be low-light adapted with values of I_k between 0.5 and 35 µmol photons $m^{-2}\,s^{-1}$ (Cota, 1985; Kuhl et al., 2001; Rysgaard et al., 2001). Based on continuously measured light levels under the ice and the I_k value, the primary producers appear to be light saturated for 75 % of the day below the snow-covered ice. From the PAR measurements and the derived model fit to the measured O_2 fluxes (Fig. 5, $R^2 = 0.923$) it was possible to estimate the net O_2 flux throughout several days including periods of insufficient turbulent mixing (Fig. 7). Because the primary producers were light saturated for most of the day, other variables could potentially control ice algae production. Gradinger (2009) found that nutrients were the major limiting factors for sea ice production while others suggest that transient photoinhibition could occur at higher PAR levels (Kuhl et al., 2001; Rysgaard et al., 2001) or that high salinities may reduce primary production (Mock and Gradinger, 1999; Mock et al., 2003; Manes and Gradinger, 2009).

Our GPP rates are supported by three recent studies at comparable sites in southwest Greenland by Mikkelsen et al. (2008), Søgaard et al. (2010), and Søgaard et al. (2011) who estimated maximum GPP rates using the ^{14}C tracer method where ice cores were melted and incubated ex situ. The first two studies were conducted in March through April and the third was conducted parallel with our eddy correlation measurements at a location approximately 100 m away from the eddy correlation site. All three studies gave similar maximum GPP rates of 1.75, 1.39, and 1.46 mmol $O_2\,m^{-2}\,d^{-1}$ (assuming a 1:1 ratio of C:O_2 for comparison purposes), respectively, which compare well with our estimate of 1.76 mmol $O_2\,m^{-2}\,d^{-1}$. The average GPP rates in March varied between the studies from 0.07 mmol $O_2\,m^{-2}\,d^{-1}$ (Søgaard et al., 2010) to 1.75 mmol $O_2\,m^{-2}\,d^{-1}$ (Mikkelsen et al., 2008) and our measurement of average GPP falls within this range (0.69 mmol $O_2\,m^{-2}\,d^{-1}$). However, the average GPP rate determined at the same time and location by Søgaard et al. (2011) (0.30 mmol $O_2\,m^{-2}\,d^{-1}$) was lower than our rate. Given the differences in methods we are not surprised by these differences; a point that is further confirmed by bacterial production rates by Søgaard et al. (2010) and Søgaard et al. (2011) using the ^3H thymidine incorporation

BGD
8, 11255–11284, 2011

method. The estimated respiration rates from ^{3}H incubations, which exclude microalgal respiration and involve a number of assumptions that vary significantly in the literature (see Søgaard et al., 2010), of −0.16 and −0.21 mmol O_2 m^{-2} d^{-1}, respectively, were an order of magnitude less than the respiration rate of −2.13 mmol O_2 m^{-2} d^{-1} by eddy correlation. We believe that these rates are highly dependent on the method used and that to some degree the differences are caused by the intrusive nature of slurry incubations in altering important parameters such as O_2, nutrients, and salinity and their distributions within the ice. Further, tracer incubations and eddy correlation may very well integrate the activity of different sections of the sea ice. These differences need further investigation as they have significant implications for determining carbon turn-over in sea ice.

In summary, the combined temperature and O_2 eddy correlation flux measurements made it possible to evaluate and separate O_2 exchange rates at the ice-water interface due to biological production and respiration from that caused by melting. In the future these rates may be further elucidated by eddy correlation salt fluxes for which fast and reliable sensors are available. We see eddy correlation measurements as an important tool in future studies of sea ice metabolism as it represents the closest we can currently come to truly in situ measurements.

Acknowledgements. This study received financial support from the Danish Agency for Science, Technology and Innovation; the Canada Excellence Research Chair (CERC) program; and the National Science Foundation, Chemical Oceanography, grant OCE-0536431. The study is a part of the Greenland Climate Research Center's activities (GCRC6507).

BGD
8, 11255–11284, 2011

References

Arrigo, K. R.: Primary Production in Sea Ice, in: Sea Ice, an introduction to its Physics, Chemistry and Biology, edited by: Thomas, D. N. and Dieckmann, G. S., Blackwell Publishing, Oxford 402 pp., 2003.

Berg, P. and Huettel, M.: Monitoring the seafloor using the noninvasive eddy correlation technique, Oceanography, 21, 164–167, 2008.

Berg, P., Roy, H., Janssen, F., Meyer, V., Jorgensen, B. B., Huettel, M., and de Beer, D.: Oxygen uptake by aquatic sediments measured with a novel non-invasive eddy correlation technique, Mar. Ecol. Prog. Ser., 261, 75–83, 2003.

Berg, P., Roy, H., and Wiberg, P. L.: Eddy correlation flux measurements: The sediment surface area that contributes to the flux, Limnol. Oceanogr., 52, 1672–1684, 2007.

Berg, P., Glud, R. N., Hume, A., Stahl, H., Oguri, K., Meyer, V., and Kitazato, H.: Eddy correlation measurements of oxygen uptake in deep ocean sediments, Limnol. Oceanogr. Meth., 7, 576–584, 2009.

Brand, A., McGinnis, D. F., Wehrli, B., and Wuest, A.: Intermittent oxygen flux from the interior into the bottom boundary of lakes as observed by eddy correlation, Limnol. Oceanogr., 53, 1997–2006, 2008.

Cole, J. J., Pace, M. L., Carpenter, S. R., and Kitchell, J. F.: Persistence of net heterotrophy in lakes during nutrient addition and food web manipulations, Limnol. Oceanogr., 45, 1718–1730, 2000.

Cota, G. F.: Photoadaptation of high Arctic ice algae, Nature, 315, 219–222, 1985.

Crusius, J., Berg, P., Koopmans, D. J., and Erban, L.: Eddy correlation measurements of submarine groundwater discharge, Mar. Chem., 109, 77–85, 2008.

Eicken, H.: From the microscopic, to the macroscopic, to the regional scale: Growth, microstructure and properties of sea ice, in: Sea Ice, An Introduction to its Physics, Chemistry and Biology, edited by: Thomas, D. N. and Dieckmann, G. S., Blackwell Publishing, Oxford, 402 pp., 2003.

Fenchel, T. and Glud, R. N.: Benthic primary production and O_2-CO_2 dynamics in a shallow-water sediment: spatial and temporal heterogeneity, Ophelia, 53, 159–171, 2000.

Fofonoff, N. and Millard, R.: Algorithm for computation of fundamental properties of seawater, UNESCO Technical Papers in Marine Science, No. 44, 1983.

Glud, R. N., Rysgaard, S., and Kuhl, M.: A laboratory study on O_2 dynamics and photosyn-

BGD
8, 11255–11284, 2011

thesis in ice algal communities: Quantification by microsensors, O_2 exchange rates, ^{14}C incubations and a PAM fluorometer, Aquat. Microb. Ecol., 27, 301–311, 2002.
Glud, R. N., Woelfel, J., Karsten, U., Kuhl, M., and Rysgaard, S.: Benthic microalgal production in the Arctic: Applied methods and status of the current database, Bot. Marin., 52, 559–571, 2009.
Glud, R. N., Berg, P., Hume, A., Batty, P., Blicher, M. E., Lennert, K., Rysgaard, S.: Benthic oxygen exchange across hard-bottom substrates quantified by eddy correlation in a sub-Arctic fjord, Mar. Ecol. Prog. Ser., 417, 1–12, 2010.
Gosselin, M., Legendre, L., Therriault, J.-C., Demers, S., Rochet, M.: Physical control of the horizontal patchiness of sea ice microalgae, Mar. Ecol. Prog. Ser., 29, 289–298, 1986.
Gradinger, R.: Sea-ice algae: Major contributions to primary production and algal biomass in the Chukchi and Beaufort Seas during May/June 2002, Deep-Sea Res. Pt. II, 56, 1201–1212, 2009.
Harvey, A. H.: Properties of Ice and Supercooled Water In: CRC Handbook of Chemistry and Physics 92nd Edn., edited by: Lide, D. R., CRC Press, Boca Raton, FL., 2656 pp., 2010.
Hume, A. C., Berg, P., and McGlathery, K. J.: Dissolved oxygen fluxes and ecosystem metabolism in an eelgrass (*Zostera marina*) meadow measured with the eddy correlation technique, Limnol. Oceanogr., 56, 86–96, 2011.
Kuhl, M., Glud, R. N., Borum, J., Roberts, R., and Rysgaard, S.: Photosynthetic performance of surface-associated algae below sea ice as measured with a pulse amplitude-modulated (PAM) fluorometer on O_2 microsensors, Mar. Ecol. Prog. Ser., 223, 1–14, 2001.
Kundu, P. K. and Cohen, I. M.: Fluid Mechanics, 4th Edn., Academic Press, 2008.
Kuwae, T., Kamio, K., Inoue, T., Miyoshi, E., and Uchiyama, Y.: Oxygen exchange flux between sediment and water in an intertidal sandflat, measured in-situ by the eddy-correlation method, Mar. Ecol. Prog. Ser., 307, 59–68, 2006.
Lorrai, C., McGinnis, D. F., Berg, P., Brand, A.: Application of oxygen eddy correlation in aquatic systems, J. Atmos. Oceanic. Technol., 27, 1533–1546, 2010.
Manes, S. S. and Gradinger, R.: Small scale vertical gradients of Arctic ice algal photophysiological properties, Photosynth. Res., 102, 53–66, 2009.
McGinnis, D. F., Berg, P., Brand, A., Lorrai, C., Edmonds, T., and Wuest, A.: Measurements of eddy correlation oxygen fluxes in shallow freshwaters: Towards routine applications and analysis, Geophys. Res. Lett., 35, 1–5, 2008.
McMinn, A. and Ashworth, C.: The use of oxygen microelectrodes to determine the net pro-

BGD
8, 11255–11284, 2011

duction by an Arctic sea ice algal community, Antarctic Sci., 10, 39–44, 1998.
McMinn, A., Ryan, K. G., Ralph, P. J., and Pankowski, A.: Spring sea ice photosynthesis, primary production and biomass distribution in eastern Antarctica, 2002–2004, Mar. Biol., 151, 985–995, 2007.
McMinn, A., Pankowskii, A., Ashworth, C., Bhagooli, R., Ralph, P., and Ryan, K.: In situ net primary productivity and photosynthesis of Antarctic sea ice algal, phytoplankton and benthic algal communities, Mar. Biol., 157, 1345–1356, 2010.
McPhee, M. G.: Turbulent heat flux in the upper ocean under sea ice, J. Geophys. Res., 97, 5365–5379, 1992.
McPhee, M. G., Morison, J. H., and Nilsen, F.: Revisiting heat and salt exchange at the ice-ocean interface: Ocean flux and modeling considerations, J. Geophys. Res., 113, C06014, doi:10.1029/2007JC004383, 2008.
Mikkelsen, D. M., Rysgaard, S., and Glud, R. N.: Microbial composition and primary production in Arctic se ice: A seasonal study from Kobbefjord (Kangerluarsunnguaq), West Greenland, Mar. Ecol. Prog. Ser., 368, 65–74, 2008.
Mock, T. and Gradinger, R.: Determination of Arctic ice algal production with a new in situ incubation technique, Mar. Ecol. Prog. Ser., 177, 15–26, 1999.
Mock, T., Kruse, M., and Dieckmann, G. S.: A new microcosm to investigate oxygen dynamics at the sea ice-water interface, Aquat. Microb. Ecol., 30, 197–205, 2003.
Platt, T., Gallegos, C. L., and Harrison, W. G.: Photoinhibition of photosynthesis in natural assemblages of marine phytoplankton, J. Mar. Res., 38, 687–701, 1980.
Shirasawa, K., Ingram, R. G., and Hudier, E. J. J.: Oceanic heat fluxes under thin sea ice in Saroma-ko Lagoon, Hokkaido, Japan, J. Mar. Sys., 11, 9–19, 1997.
Smith, R. E. H., Anning, J., Clement, P., and Cota, G.: Abundance and production of ice algae in Resolute Passage, Canadian Arctic. Mar. Ecol. Prog. Ser., 48, 251–263, 1988.
Søgaard, D. H., Kristensen, M., Rysgaard, S., Glud, R. N., Hansen, P. J., and Hilligsoe, K. M.: Autotrophic and heterotrophic activity in Arctic first-year sea ice: Seasonal study from Malene Bight, SW Greenland, Mar. Ecol. Prog. Ser., 419, 31–45, 2010.
Suzuki, Y., Kudoh, S., and Takahashi, M.: Photosynthetic and respiratory characteristics of an Arctic ice algal community living in low light and low temperature conditions, J. Mar. Syst., 11, 111–121, 1997.
Rysgaard, S., and Glud, R. N.: Anaerobic N_2 production in Arctic sea ice, Limnol. Oceanogr., 49, 86–94, 2004.

BGD
8, 11255–11284, 2011

Rysgaard, S., Kuhl, M., Glud, R. N., Hansen, J. W.: Biomass, production and horizontal patchiness of sea ice algae in a high-Arctic fjord (Young Sound, NE Greenland), Mar. Ecol. Prog. Ser., 223, 15–26, 2001.

Rysgaard, S., Glud, R. N., Sejr, M. K., Blicher, M. E., and Stahl, H. J.: Denitrification activity and oxygen dynamics in Arctic sea ice, Polar Biol., 31, 527–537, 2008.

Widell, K., Fer, I., and Haugan, P. M.: Salt release from warming sea ice, Geophys. Res. Lett., 33, L12501, doi:10.1029/2006GL026262, 2006.

BGD

8, 11255–11284, 2011

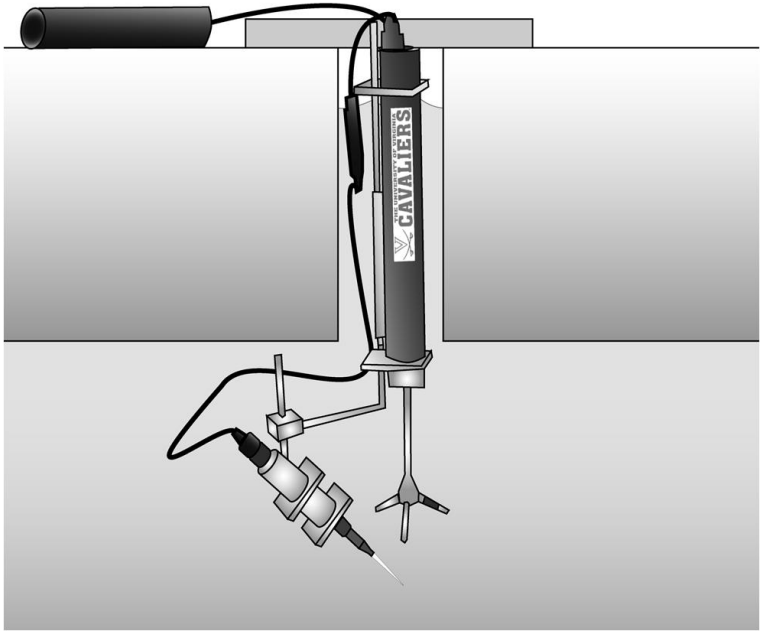

Fig. 1. Eddy correlation instrument deployed under sea ice through a rectangular-shaped hole and secured with a T bar at the ice-air interface. The instrument may freeze into the ice but the power supply (top left) and communication port (top center) remained accessible from above.

BGD
8, 11255–11284, 2011

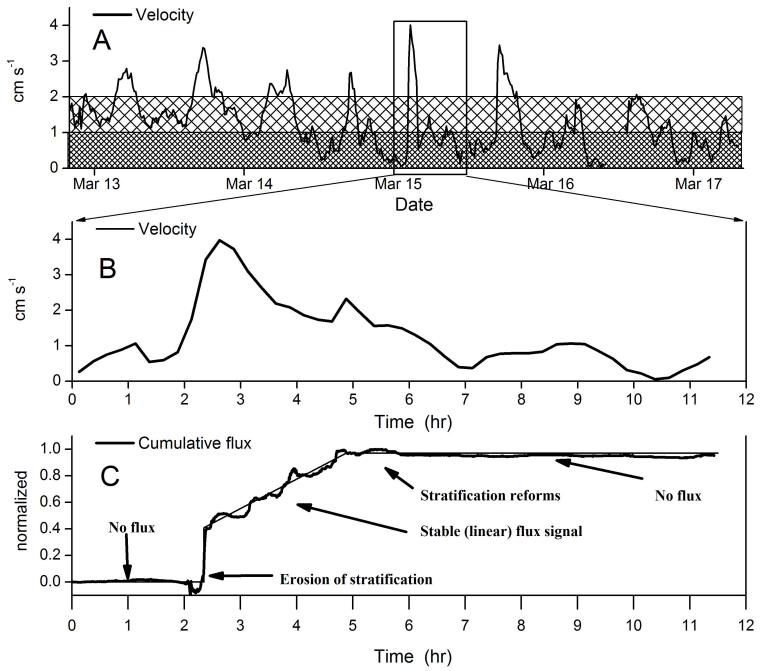

Fig. 2. **(A)** is the mean current velocity measured 22 cm below the ice-water interface over 4.5 d. The dark shaded region (<1 cm s^{-1}) represents conditions where density stratification in the water column appeared to be persistently present while the lightly shaded region (1–2 cm s^{-1}) represents conditions where stratification was occasionally observed. The presence of stratification was evaluated by examining the mean velocity and the stability and linearity of the cumulative flux signal. **(B)** shows a magnified 12 h segment of the velocity data in **(A)**. **(C)** shows that during this segment the flux is strongly dependent on stratification. The magnitude of the vertical rise at hour 2.3, when stratification eroded, was not indicative of any true flux and therefore was not included in the flux measurements.

BGD
8, 11255–11284, 2011

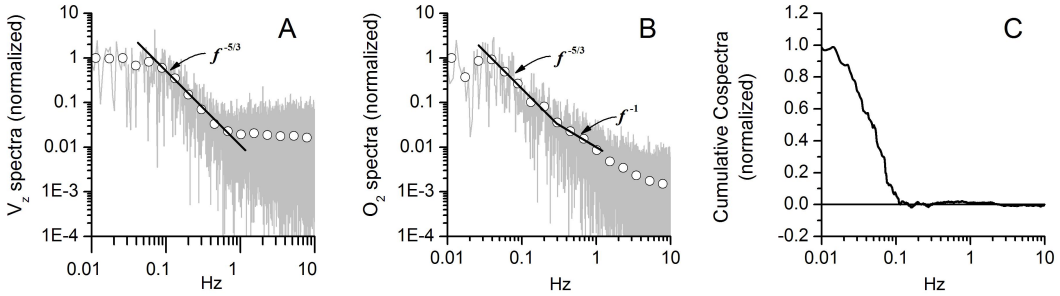

Fig. 3. Typical spectra for current-driven turbulent flow under sea ice (current velocity: 1.86 cm s^{-1}). **(A)** and **(B)** show the normalized spectra of the vertical velocity and the O_2 concentration, respectively. The −5/3 slope is indicative of well-developed turbulence and represents the inertial subrange where inertial forces dominate transport, according to Kolmogorov's theory of turbulence. The −1 slope at higher frequencies in the O_2 spectrum indicates the transport of O_2 by both viscous and convective forces. **(C)** shows the normalized cumulative cospectra of O_2 and vertical velocity and reveals that eddies with frequencies $<\sim 0.1$ Hz contributed most of the vertical turbulence-driven O_2 transport.

BGD
8, 11255–11284, 2011

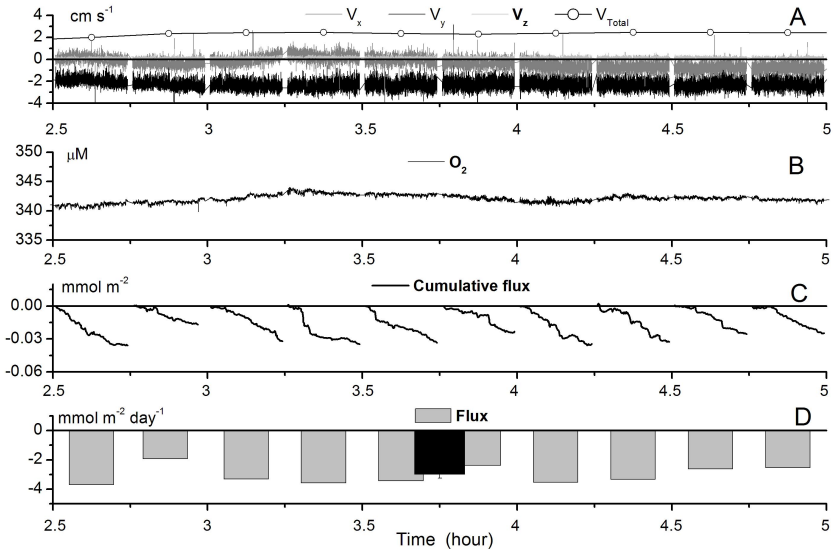

Fig. 4. A typical example of eddy correlation data measured in 0.25 h segments 22 cm below the ice-water interface through 2.5 h. **(A)** shows the x, y, and z components of the velocity at 16 Hz and the mean current velocity. **(B)** shows the corresponding O_2 concentration at 16 Hz. **(C)** shows the cumulative flux calculated for each 0.25 h segment and **(D)** is the average O_2 flux averaged across each 0.25 h segment. The black bar is the O_2 flux averaged across 2.5 h where the error bar represents the standard error.

BGD
8, 11255–11284, 2011

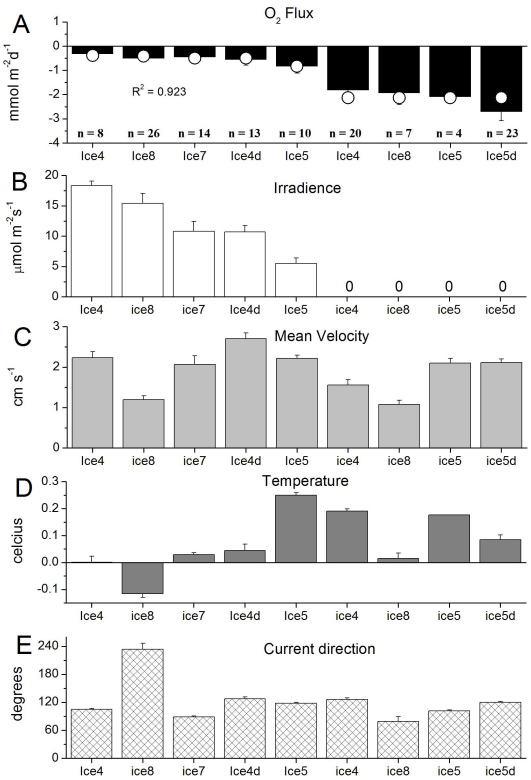

Fig. 5. Averaged O_2 fluxes for periods with well-developed turbulence under the ice-water interface are shown in **(A)**, where n is the number of 0.25 h data segments included in the flux extractions. The open circles in **(A)** represent the flux determined by fitting Eqs. 3 and 4 ($R^2 = 0.923$) to the averaged fluxes. **(B, C, D)** and **(E)** show the irradiance, mean current velocity, temperature and current angle over each 0.25 h data segment, respectively. All error bars represent standard errors.

BGD
8, 11255–11284, 2011

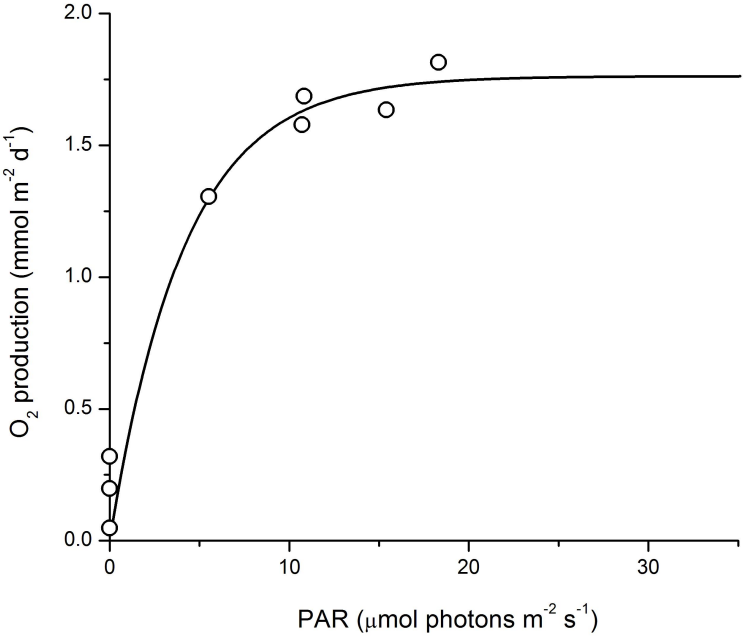

Fig. 6. P/I curve calculated by fitting Eqs. 3 and 4 ($R^2 = 0.923$) to the averaged fluxes in Fig. 5A. The open circles represent the GPP determined from the averaged fluxes in Fig. 5A. This P/I curve had an I_k value of 4.2 μmol photons m^{-2} s^{-1} which represents the point where light saturation begins to occur.

BGD
8, 11255–11284, 2011

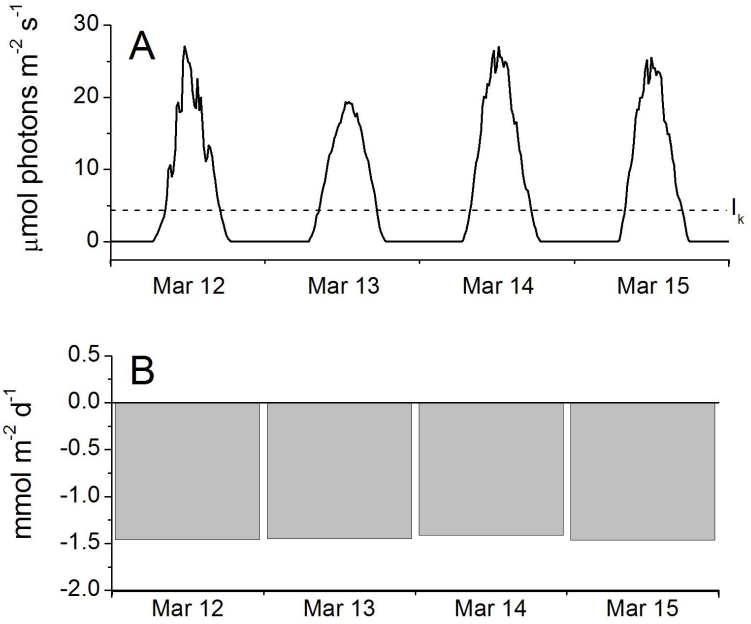

Fig. 7. (A) shows four days of ice irradiance values measured immediately below the ice. The dashed line is the I_k value determined from the P/I curve and indicates that light saturation is present over much of the daylight hours. **(B)** shows the 24 h integrated O_2 fluxes calculated from the irradiances in **(A)** and Eqs. 3 and 4.

BGD
8, 11255–11284, 2011

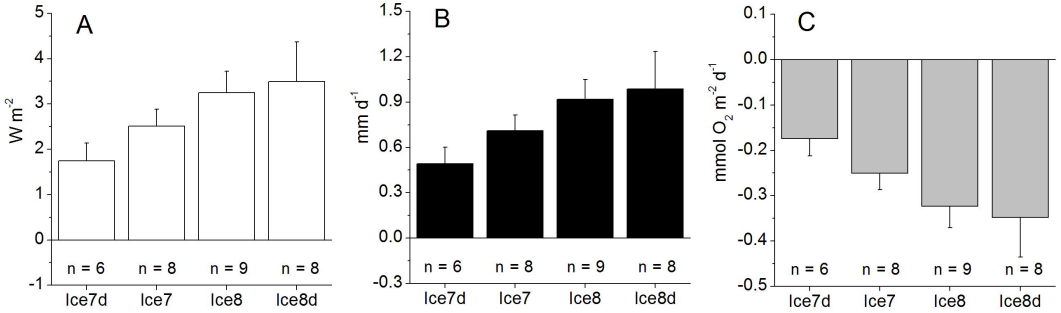

Fig. 8. (A) shows the averaged heat fluxes for periods with well-developed turbulence under the ice-water interface. The maximum potential ice melt rate derived from the heat flux is shown in **(B)** and the maximum O_2 flux calculated from this melt rate is shown in **(C)**. The *n* is the number of 0.25 h measuring periods and error bars represent standard errors.

BGD
8, 11255–11284, 2011

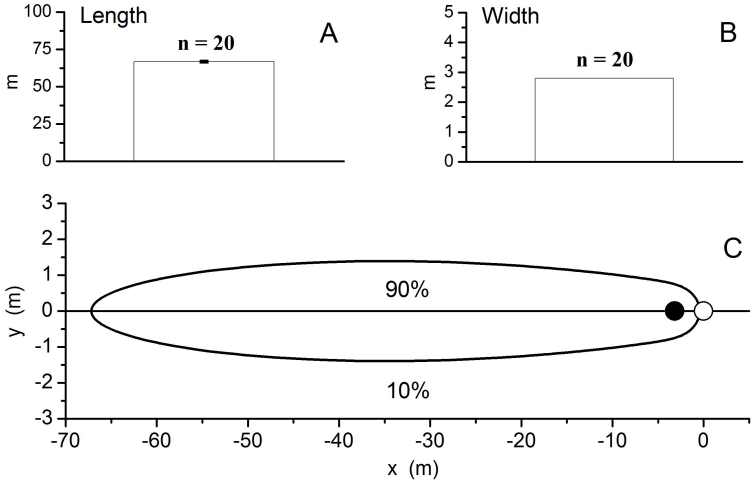

Fig. 9. The footprint length, width and shape are shown in **(A, B, and C,)** respectively. The error bars represent standard error and n is the number of 0.25 h measuring periods. **(C)** shows the footprint or the area that contributes 90 % of the flux (note the difference in axis scales). The open circle represents location of the eddy correlation instrument and the solid circle indicates the point of maximum flux contribution.

BGD
8, 11255–11284, 2011

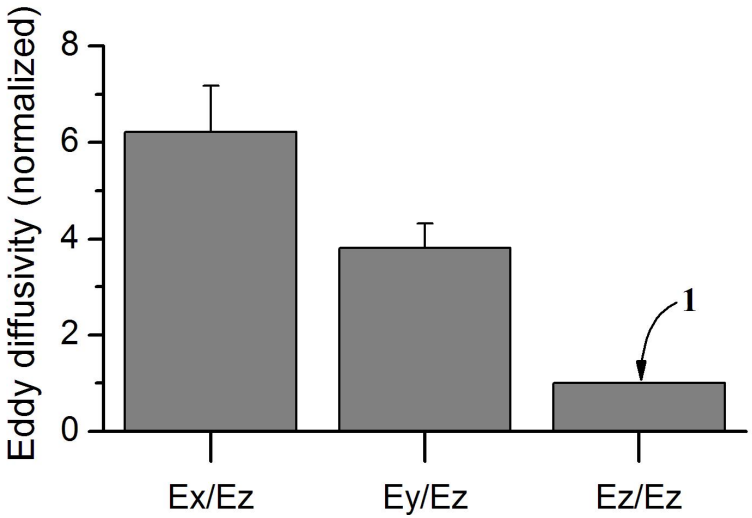

Fig. 10. Level of anisotropy in the turbulent flow below the sea ice, as reflected in the ratios between the eddy diffusivities (Ex, Ey, and Ez) in the x, y, and z directions

BGD
8, 11255–11284, 2011